Article:
Farshchi, A, Bayly, A and Bayly, AE (2019) The structure of spray-dried detergent powders. Powder Technology, 355. pp. 738-754. ISSN: 0032-5910

https://doi.org/10.1016/j.powtec.2019.06.049

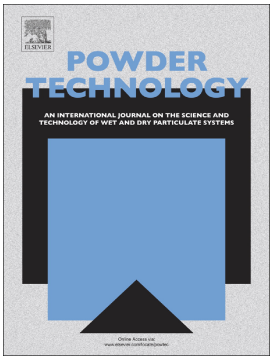

The structure of spray-dried detergent powders

Amin Farshchi, Ali Hassanpour, Andrew E. Bayly

PII: S0032-5910(19)30492-9
DOI: https://doi.org/10.1016/j.powtec.2019.06.049
Reference: PTEC 14453

To appear in: *Powder Technology*

Received date: 26 September 2018
Revised date: 18 June 2019
Accepted date: 30 June 2019

Please cite this article as: A. Farshchi, A. Hassanpour and A.E. Bayly, The structure of spray-dried detergent powders, Powder Technology, https://doi.org/10.1016/j.powtec.2019.06.049

The structure of spray-dried detergent powders

Amin Farshchi* a.farshchi@leeds.ac.uk, Ali Hassanpour, Andrew E. Bayly*

a.e.bayly@leeds.ac.uk

School of Chemical and Process Engineering, University of Leeds, Leeds, LS2 9JT, UK

*Corresponding authors.

Abstract:

The complex multi-scale structure of spray-dried detergent granules has been characterized using a range of techniques including microscopy, wide-angle and small-angle X-ray scattering and X-ray microtomography. Four simple model formulations based on linear alkyl benzene sulphonate (NaLAS) and sodium sulphate were used to probe the influence of initial slurry water content and sodium silicate on the structure. The structure can be viewed as a porous matrix consisting of liquid crystalline NaLAS, sodium sulphate and binder in which large crystals of sodium sulphate are embedded. These large crystals were initially undissolved in the slurry and are consequently reduced in number in the product made from higher water content slurry. The both slurry water content and sodium silicate changed the polymorphs, and the *d*-spacing of the lamellae. The surface micro-structure and particle morphology can also be significantly affected with the high initial water content; particles having a distinct agglomerated and blistered structure.

1. Introduction

A laundry detergent powder is a formulated mixture of ingredients which predominantly includes surfactants, builders, bleaches, and fillers. In the vast majority of the detergent granules the most important functional component is the sodium salt of linear alkylbenzene sulphonate (NaLAS). The NaLAS is added to the composition via granules which typically form the largest single added component in the formulation; consequently this component is

responsible for the physical properties and many performance related characteristics of the formulation such as caking tendency and dissolution rate. Globally, the vast majority of detergent powders are manufactured either by spray drying or by mechanical agglomeration/granulation; of these two processes, spray drying is the most widely used and produces a low-density and free-flowing powder by drying droplets of atomized detergent slurry.

A typical detergent slurry fed to a spray dryer is a multiphase mixture and is composed of a continuous aqueous phase saturated with respect to inorganic salts, in which dispersed, liquid crystalline phase(s) of surfactants along with inorganic crystals and air bubbles are suspended (Stewart et al., 2011). Upon spray drying, the liquid phases are transformed into a dried, porous matrix which binds the suspended solids together and entraps air. As will be shown, this matrix is itself a porous, composite structure of dehydrated liquid crystalline surfactant and sub-micron scale crystallites of inorganic salts and binder, if present. The structure of spray-dried detergent powders, however, has not been well characterised or reported, at least in the publically accessible literature. (Walton and Mumford, 1999) studied the morphological properties of single detergent granules produced using a single droplet drying apparatus, though the majority of this research was concerned with the droplet drying of single-component solutions, *e.g.* sodium silicate, sodium sulphate and alkyl benzene sulphonate, at various concentration and temperatures. In the case of multi-component detergent systems, (Griffith et al., 2007) investigated the evolution of the internal micro-structures, *e.g.* porosity, in drying detergent pastes, through the application of nuclear magnetic resonance (NMR). Most recently, there have also been a few studies investigating the effect of operating conditions, *e.g.* nozzle configuration, air drying temperature (Francia et al., 2015) and nozzle height (Francia et al., 2016a), on the formation of detergent agglomerates in counter-current spray dryers. However, none of the above-mentioned studies

provides a detailed understanding of the multiscale structure of detergent powders or investigates the effect of formulation on these structures and it is this gap in knowledge that this paper aims to address.

In contrast to spray-dried particles, the structure of agglomerated detergent particles has received slightly more attention (Boerefijn et al., 2007, Van Dalen et al., 2011). Van Dalen et al. (2011) studied the structure of detergent agglomerates using several imaging techniques including X-ray microtomography, Fourier Transform Infrared microscopy and Scanning Electron Microscopy (SEM). The study was focused on the capability of correlative microscopy combined with other image analysis techniques to characterize the structure of detergent powders. Detergent agglomerates are formed using a surfactant paste as a binder between solid particles and have a density which is significantly higher than spray dried granules, therefore, the structure and morphology of these agglomerates is considerably different from that of spray-dried powders. Despite this difference, the work highlights the value of understanding the spatial distribution of components in the granules.

The distribution of components in spray-dried granules comes from the initial phase composition, the phase and colloidal structures present, and their subsequent transformation during drying. The evolution of porosity, both on a micro and a macro-scale, is important to spray-dried powder properties. Spray-dried powders normally possess a porous structure composed of gas-filled pores/voids, which can be either closed (without any connection to the exterior) or open to the particle surface (Rouquerol et al., 1999). Particle porosity has been demonstrated to be a decisive factor that can influence the functional properties of spray-dried granules, by lowering their bulk density, or by enhancing the dissolution rate of dried particles (Ansari and Stepanek, 2008, Juppo and Yliruusi, 1994). For detergents, specifically, the typical process conditions used can expose the particles to temperatures above their boiling point (Ali et al., 2017), and if the droplet temperature also exceeds its boiling point,

i.e. insufficient evaporative cooling, then boiling within the droplet would be anticipated (Charlesworth and Marshall, 1960); The steam generated during puffing can inflate the granules and lead to hollow structures (Hecht and King, 2000, Walton, 2002).

The structure and micro-scale porosity created by the drying and solidification of the liquid phases are determined by composition, initial structure and by the process conditions they experience. In a typical spray-dried system, the drying rate is very high and this can lead to non-equilibrium phase behaviour and structures, *e.g*. amorphous rather than crystalline solids, meta-stable polymorphs. In the case of spray-dried detergent powders, the structure of the dried matrix and the phases present have not been investigated. The crystallisation behaviour and crystal size of dissolved inorganics; the changes to the liquid crystalline phases on drying; the creation of micro-scale porosity and the spatial distribution of these phases are all unreported.

The fraction, composition and structure of the aforementioned phases in a multi-component formulation, and more particularly their spatial arrangements, will have a profound effect on handling and functional properties of detergent powders. To the best of our knowledge most previous studies are concerned with the structure of detergent agglomerates manufactured by non-tower agglomeration processes, while the structure of spray-dried detergent powders has not received fundamental attention. It is evident that, due to the complexity of the system, a spray-dried detergent powder's structure is difficult to elucidate and explain. However, in order to successfully design a complex-structured powder which is efficiently capable of satisfying consumer requirements, *e.g.* good flowability, good storage stability and rapid dissolution, a deeper understanding of the structure is required.

This study is focused on developing a better fundamental understanding of the relationship between the slurry formulation and structure of these powders, which is important for particle

design and engineering. Four simple model formulations based on linear alkylbenzene sulphonate (LAS) and sodium sulphate were used to probe the influence of initial slurry water content and binder, sodium silicate (SiO_2:$_nNa_2O$), on the structure. (Sodium silicate is the most common binder used in spray-dried detergent compositions and as well as strengthening the granule and improving flowability and storage properties, it also has a number of wash performance benefits such as soil suspension, alkalinity, buffering and corrosion inhibition.) The spray-dried formulations were produced using process conditions which were typical of the production scale and, as far as possible, kept the same between formulations. The structure and morphology, both external and internal of the powders, were examined using several techniques including SEM and X-ray microtomography. The internal micro-structures, *e.g.* cross sections of particle wall, were further investigated using SEM of microtomed sections which enabled smaller scale structures to be seen. The phase structures were also investigated, *e.g.* self-assembled nano-structures of surfactant molecules and polymorphs of inorganic salts. Small-angle X-ray scattering (SAXS) was used to probe the self-assembled structures of NaLAS within the powder and the existence of polymorphs of sodium sulphate was examined at smaller length scales using a wide-angle X-ray scattering (WAXS) technique.

2. Material and methods

2.1. Materials

Four model formulations of detergent granules were produced with a pilot-scale spray dryer by Procter & Gamble. The tower was designed and operated to give drying conditions that are representative of larger scale production facilities. Typical process conditions were used and, as far as possible, these were kept consistent between formulations. Detergent slurries with a temperature of 85°C were introduced into the spray dryer operating with an inlet air

temperature of 280°C. The flow rate of slurry was altered to achieve the target product moisture content. The airflow rates were constant during and between each production run. The atomization conditions were kept constant in all the low-water content formulations (see below for formulation details), and adjusted to give a similar mean product particle size for the high water formulation which had a lower viscosity and was therefore easier to atomise. These input conditions and operating strategy lead to an exhaust temperature of ~100°C in all of the runs. Product samples were only taken when the production had achieved a steady state.

All spray-dried powders contained the sodium salt of linear alkylbenzene sulphonate, NaLAS, with a molecular weight of 340 g/mol, and sodium sulphate. However, their formulation varied depending on either the initial water content (30 or 63 wt% on a wet basis) of the slurry or the addition of sodium silicate with molar-ratios of 1.6 and 2.35 SiO_2:Na_2O. The details of the four compositions are shown in Table 1. The abbreviations used to identify the formulations are used throughout this paper: **LW**: low-water content slurry; **HW**: high-water content slurry; **LW+1.6R**: low-water content slurry containing 1.6 SiO_2:Na_2O ratio sodium silicate; **LW+2.35R**: low-water content slurry containing 2.35 SiO_2:Na_2O ratio. The dried composition of LW and HW formulations was identical and the dried surfactant level was identical, 19.5 %, in all formulations.

2.2. Slurry Phase Compositions

As mentioned in the introduction, detergent slurry can be considered as a multi-component colloidal system in which crystals of inorganic salts along with liquid crystalline phases of

surfactant molecules are suspended in a continuous aqueous phase saturated with the inorganic salts. The amount of sodium sulphate remaining undissolved in the detergent slurries can be roughly estimated based on the solubility of sodium sulphate in water at 85°C; the solubility of sodium sulphate at this temperature is ~ 31.0 g in 100 g of water (Okorafor, 1999). Table 2 shows an estimated level of undissolved salts and the corresponding composition of the liquid matrix, *i.e*. both liquid crystalline and aqueous phases, in which the undissolved sodium sulphate is suspended. For this estimate, the influence of sodium silicate on the solubility of sulphate in the aqueous phase is not taken into account. Both the relative amount and composition of the liquid matrix is governed by the water content of the slurries. The higher the concentration of water, the greater the amount of dissolved sodium sulphate, and consequently the higher the ratio of sodium sulphate to NaLAS within the liquid matrix. This is shown in Table 2, the liquid matrix of high-water content detergent slurry (HW), containing 63 wt% water, has a sodium sulphate to NaLAS ratio of 21.8:8.0, or 2.725:1, whereas the low-water content slurry (LW), containing 30% water, has dramatically reduced ratio of 17.6:25.7, or 0.685:1. The fraction of the liquid matrix is significantly lower for the LW slurry 52.9 % compared with the 89.7 % for the HW slurry. The extent of these phase composition changes in the slurry are reflected in the dried matrix composition of resulting spray-dried powders and consequently are highlighted here as they are a critical consideration in the discussion that will follow when interpreting the microscopic observation.

2.3. Microscopic observations

The morphologies of three representative sieve fractions 150-180, 300-350 and 600-710 µm, were evaluated using scanning electron microscopy (SEM). Prior to SEM observation, the samples were sputter coated with an ultra-thin coating of gold to inhibit charging during SEM examination. A microtome sectioning technique was also utilised to examine the internal structure of the granules. Prior to microtoming, the samples were embedded with an epoxy resin (Epofix cold mounting resin, Struers) in plastic moulds and cured over 24 hours. The blocks of resin containing samples were then polished using an ultra-microtome equipped with a diamond knife. The polished blocks were subsequently mounted and coated before microscopic observation. In order to determine the interconnectivity of pores in SEM micrographs, the pores were segmented using an interactive thresholding tool in the Avizo software package. The connected sets of objects were then labelled with the same colour, based on pixel connectivity, by the Lable image tool in Avizo. The processed image is presented using a cyclic colour map such that pores in close proximity are likely to be displayed in a different colour.

2.4. Shape characterization of particles by Malvern Morphologi G3

Particle size distribution and shape analysis were carried out using an imaging based system, the Malvern Morphologi G3 (Malvern Instrument, Malvern, UK). Prior to particle size measurements, representative samples were obtained using a sample splitter, these samples were then dispersed and distributed as a monolayer onto a sample stage using the automated dispersion unit. A dispersion pressure of 1.2 bar was chosen to avoid particle attrition. For the particle size measurements, particle imaging was carried out using 2.5× magnification lens (13µm–1000µm resolution range). For the shape characterization, 5 times magnification (6.5µm - 420µm) was used. The 2-dimensional images of each particle were used to produce size and shape distributions of the sample. Amongst the shape parameters, circularity is

sensitive to both changes in overall shape and edge roughness (Hafid et al., 2016). High sensitivity circularity, *HSC*, defined in eq. (1) below was chosen as a suitable shape parameter. *HSC* is an indicator of the closeness to a perfect circle and can be written as follows:

$$HSC = circularity^2 = 4\pi \times \frac{area}{perimeter^2} \qquad (1)$$

HSC values ranges between 0, highly irregular, to 1 a perfect sphere. Further information can be found in (Li et al., 2008) and (Ulusoy and Kursun, 2011).

2.5. X-ray micro-computed tomography (X-ray micro-CT)

X-ray microtomography has proved to be a non-destructive and useful technique to provide detailed 3D visualisation of internal structures and morphologies of spray-dried powders (Gamble et al., 2016). In this study, the internal structure of spray-dried detergent powders were qualitatively examined using a Phoenix Nanotom CT scanner (GE Measurement and Control, US). This provides qualitative and quantitative analysis of the distribution of high density and low-density phases within the powder.

Sieved size cuts of the sample powders were loaded in a plastic (polypropylene) tube (internal diameter 2 mm, height 8.5 mm), which was subsequently mounted on a rotating stage between an X-ray source and X-ray detector. X-ray source settings were 80 kV and 120-140 μA, and a total of 1440 angular projections were acquired at 0.25° angular intervals in a single 360 ° rotation. Three-dimensional volumes were reconstructed using the VGStudio software package. The original volume was cropped and a cube (1500×1500×1500 μm) was created for further image processing (Fig. 1). For 300 – 350 um particles, there were typically 100–120 particles in this volume. To improve the 3D data visualisation, a number of different image processing tools including filtration and segmentation, were applied to the X-ray

micrograph data using the Avizo software package. A non-local mean algorithm was applied to the grey scale projections to reduce image noise. The segmentation of highly dense regions, corresponding to initially undissolved sodium sulphate particles, from the matrix was conducted using an interactive thresholding tool in Avizo. The resulting 3D rendered volume of the segmented region was then used to determine the quantity of undissolved sodium sulphate and estimate the matrix composition. The true density of anhydrous sodium sulphate (2.66 g/cm^3) was used to determine the mass of the rendered volume corresponding to undissolved salts. The total mass of detergent powders within the volume of interest was estimated using from tapped bulk density measurements. Tapped density were measured on 50 ml samples with 5 minute tapping duration on a Tapped Density Tester (Series JV 2000; Copley Scientific Limited,Nottingham, UK).

The segmentation of closed intra-particle pores, *i.e*. not connected to the inter-particle void space, from the particle matrix was conducted using an interactive Top-Hat thresholding tool and the resulting binary images were used for 3D-volume rendering and further analysis. An example of the 3D rendered intra-particle pores can be seen in Fig. 1b. The porosity (φ) was defined by the ratio of the volume of isolated pores space (V_V) to the volume of detergent powders (V_P) within the 3D reconstructed cube.

$$\varphi = \frac{V_V}{V_P} \times 100 \qquad (2)$$

Pore size distributions were obtained from this data set and the number of pores was in the region of 7000 – 15000.

Figure 1. A filtered grey scale XRT image (voxel size: 2.5 µm) showing two sides of a cubic sub-volume (1500×1500×1500µm) obtained from the original scan of 300 – 350 µm

detergent particles (a), and an example of typical 3D rendered closed intra-particulate pores within an individual granule (b).

2.6. X-ray diffraction (XRD) measurements

The existence of polymorphs of sodium sulphate was investigated by X-ray diffraction, XRD, (D8 Advance, Bruker axs, Karlsruhe, Germany) using a Cu Kα X-ray source. The samples were packed tightly in a sample holder with a 2mm indent. The scanning region of the diffraction angle was between 10 - 40° (2Θ). Surfactant structure was investigated using small-angle X-ray scattering conducted using a Xeuss 2.0 SAXS system (Xenocs, France). A Cu Kα X-ray source (λ=0.154 nm) and scatterless collimating slits were used during the experiments. The scattering vector modulus is defined in this work as $q = 4\pi/\lambda \sin(\theta)$, with 2θ being the scattering angle. The one-dimensional lattice spacing (*d*-spacing) was determined according to the Bragg equation, $d = 2\pi/q$ (Bragg and Bragg, 1913). For lamellar phases of surfactant molecules this equals to the sum of the water and alkyl chain region dimensions (Fig. 2).

Figure. 2. A typical schematic of a lamellar phase and SAXS measurement.

3. Results and discussion

3.1. Morphology and particle size distribution

The morphological characteristics of the spray-dried detergent powders were evaluated using scanning electron microscopy (SEM). As these characteristics are a function of particle size a clearer insight into the size dependent morphology can be obtained by examining sieved size fractions. Representative images of three fractions are presented here, 150-180 µm, 300-350 µm and 600-710 µm, Figures 3, 4 and 5. These fractions were selected to illustrate the characteristics of the mean/modal size and show the clear difference in morphology observed for smaller and larger particles.

Clear morphological differences can be seen between the formulations, in particular, the high-water content formulation stands out as different from the low-water content formulations. Size dependent morphology is also seen, with the level of agglomeration increasing with size as would be anticipated (Francia et al., 2015, Francia et al., 2016b). Evidence of the hollow nature of the particles is also seen in most images as holes caused by fracture of the thin shell walls are observed. The hollow morphology of the particles is not unusual in this case it is driven by steam puffing. (The morphology generated is seen clearly in the X-ray micro-CT analysis, Fig. 8, and will be discussed further in Section 3.2).

Looking at the images in more detail; the 150-180 µm particles (Fig. 3) consist of a single large primary particle, formed from a single droplet, to which smaller particles are attached. The agglomeration of smaller particles is formulation dependent. The particles from low water content slurries are almost spherical in shape and have relatively smooth surfaces; the addition of sodium silicate increases the small number of fine particles attached to the primary particle surface. In contrast, the high-water content slurries were less spherical, and slightly rougher with more open surface pores. The lower sphericity might be seen as surprising as more spherical particles are often produced with low viscosity slurries, as the surface tension draws the droplet into its equilibrium spherical shape before the rapid drying

slows the mobility of the surface and freezes the structure in a non-spherical shape. However, in this case, we are seeing agglomeration and, perhaps, some internal blistering that is leading to a slightly less spherical shape, even at these low particle sizes. These differences are more pronounced in the 300 - 350 µm fractions, which are fairly representative of mean particle sizes, (Fig. 4). In this figure the HW formulations again show a higher level of agglomeration and blistering than the other formulations. These particles are made up from a large number of smaller, hollow, particles often agglomerated around a single central particle, and as will be seen in the X-ray micro-CT results form an almost sponge like particle. Although some of the particles are clearly the result of the collision and coalescence of originally separate droplets particles, it may also be that several bubbles grow simultaneously during the drying process and that bubbles growing in the wall of the particle causes the blistered like appearance.

Figure 3. SEM micrographs of spray-dried detergent powders (150-180 µm).

Agglomeration is also seen in the low water, sodium silicate containing formulations, whereas the non-silicate containing LW formulation shows little agglomeration, this is highlighted at the highest sieve fraction measured, *i.e*. 600 to 710 µm (Fig. 5), where virtually no agglomeration is seen in the LW formulation. The morphologies of these particles also indicate, as expected for the spray drying system used, that the agglomeration seen is a result of inflight collisions rather than wall agglomeration which results in particles which resemble broken fragments of 'cake' with some angularity (Francia et al., 2015).

In general, agglomeration can occur inside the spray dryer chamber due to the collisions between fine particles, which are typically already dried, and semi-dried particles which still

have wet surfaces (Blei and Sommerfeld, 2003, Verdurmen et al., 2004). These collisions results in coalescence of the two particles, where as in collisions between two dry particles no aggregation occurs. The extent of agglomeration of spray-dried powders is therefore determined by the surface composition and the moisture content of the outermost layers of the drying droplets, as well as the collision rate. During the spray drying process, as the evaporation progresses, the droplet surface viscosity rapidly increases with a concomitant increase in solute concentration, until reaching a critical value. This viscosity is often referred to as sticky-point viscosity (10^6-10^8 Pa.s) above which further agglomeration does not take place (Walton, 2002, Goula and Adamopoulos, 2008). Consequently in cases where drying is rapid, the surface moisture concentration is rapidly reduced which results in non-sticky particles that are less likely to undergo agglomeration. The higher agglomeration in the HW versus LW formulations is therefore consistent with a longer period when the particle surfaces are still wet/sticky which would be expected for higher initial water content slurries. The presence of sodium silicate on the surface is also increasing the likelihood of agglomeration; in these formulations the initial composition of the surface, formed from the liquid phases, is 14 – 18% silicate (Table 2). Sodium silicates species are known to possess hygroscopic characteristics, and are capable of adsorbing water molecules around their silanol (Si-OH) functional groups (Asay and Kim, 2005, Leroch and Wendland, 2012). This characteristic is potentially causing an increase in surface stickiness of the partially dried particles and higher levels of agglomeration than the equivalent non-silicate formulation.

Figure 4. SEM micrographs of spray-dried detergent powders (300-350 μm).

Figure 5. SEM micrographs of spray-dried detergent powders (600-710 µm).

The degree of agglomeration is also evident in the particle size and shape factor distributions, (Fig. 6 & 7). The particle size measurements show that powders produced from high-water content slurries are significantly larger, *d*50 = 377 µm, than those produced from low-water content slurries, *d*50 = 270 µm. Whilst agglomeration is likely to be a significant contributor to this difference in size, the increased water content would be expected to lead to more bubble growth and puffing (Walton, 2002), therefore increasing the primary, pre-agglomerated, particle size versus the LW formulations.

The addition of sodium silicate with the SiO_2:Na_2O molar ratios of 1.6 and 2.35 to low-water-content slurries, however, did not result in a noticeable change in the median particle diameter d50 ~ 270 µm, although the volume percentage of larger particles in the range of 360-600 µm is slightly higher compared with those in the absence of sodium silicate. This is possibly due to the formation of agglomerates in the silicate-containing formulations (as was shown earlier in the SEM micrographs).

Figure 6. Volume-weighted particle size distributions of spray-dried powders as a function of detergent formulation. Each graph includes the probability distribution and the cumulative distribution.

The results of the SEM micrographs are reflected quantitatively in the shape factor distributions presented in Fig. 7. The high-water content formulation (HW) showed the lowest *HSC* value in all sieve fractions, the agglomeration and blistering resulting in particles with a rougher outline and *HSC* distributions which extend to lower values than the smoother, more spherical particles produced from the LW formulations. In general, in most cases, the

larger the sieve cut size, the smaller the *HSC* value. However, in the case of LW formulation, a slightly smaller *HSC* of 0.801 is seen for fine particles (150-180 μm) compared with medium-sized particles (300-350 μm), this is thought to be because the particle shape is being influenced by the size and shape of the remaining undissolved, non-spherical, sodium sulphate particles within the granule. The presence of remaining undissolved sodium sulphate particles will be discussed later in section 3.2.

Amongst the medium-sized granules, powders produced from the LW slurry showed the largest *HSC* value, 0.814, the mean *HSC* value of detergent powders decreasing to 0.774 and 0.757 on addition of sodium silicate with the SiO_2:Na_2O molar ratios of 1.6 and 2.35 respectively, probably due to the higher agglomeration level. Interestingly, a similar comparison at the highest particle size shows very similar mean HSC values (LW, 0.697; LW+1.6R, 0.708; LW+2.35R, 0.708) despite a noticeable difference in morphology seen in the SEM images. This highlights the need to be careful when interpreting shape factors.

Figure 7. Volume-weighted high sensitivity circularity, *HSC*, distributions of representative size cuts of the spray-dried detergent powders.

In summary, the external morphology of the powder is driven by puffing and agglomeration. At high water contents the puffing is more significant and there is more chance for agglomeration as the particles remain sticky for longer. Additives can also change this behaviour. Sodium silicate increases the particle agglomeration as changes in the surface properties increase the chance of agglomeration. These changes are seen qualitatively in the SEM images and quantitatively in the size and shape distributions.

3.2. Internal structures

The internal morphology and structure of the particles was studied via X-ray micro-CT and SEM imaging of microtomed sections of the particles. The microscopy enables the sub-micron structures to be investigated, whilst the microtomography gives insights into the overall internal structure at larger scales (voxel size 1.5 µm), and in particular highlights regions of different densities.

3.2.1. X-ray micro-computed tomography (micro-CT)

At the macro-scale, the internal morphology, *e.g*. vacuole size, porosity distribution, shape and spatial distribution of remaining undissolved sodium sulphate, of the spray-dried powders was examined using X-ray microtomography. Fig. 8 compares 3D reconstructed X-ray micro-CT slices, ~ 70 µm thick, taken across the centre of typical particles for two size fractions, 300-350 µm and 500-600 µm. The dark areas inside the particles indicate the intra-particle voids. The light blue, almost white, internal bodies within the particles correspond to more dense materials, *i.e.* remaining undissolved sodium sulphate. (The LW+2.35R images were very similar to the LW+1.6R images and therefore not shown.)

Figure 8. 3D central cross sections (60-70 microns thick) of spray-dried detergent powders reconstructed from X-ray micro-tomography, with voxel resolution of 2.5×2.5×2.5 µm. From 300 – 350 µm size, left hand column, and 500 – 600 µm, right hand column, sieve fractions. LW, HW and LW+1.6R formulations.

LW and LW+1.6R formulations

For the smaller sieve cut, *i.e*. 300-350 µm, of the LW and LW+1.6R formulations, one or more large vacuoles, *i.e.* relatively large intra-particle space > ~0.1 the particle diameter, can be observed inside the particles. Some particles contain a large central vacuole accompanied by small-sized voids, *i.e.* macro-pores, distributed throughout the wall. These small voids are more prevalent in the particles containing sodium silicate. The reconstructed tomographs also revealed the presence of a large number of crystals of remaining undissolved sodium sulphate (light blue regions). These crystalline particles are either non-homogeneously dispersed around the central vacuole or occupy most of the internal space of the granules as a big particle. Fig. 9a illustrates the external morphology of a typical single detergent granule produced from the LW+1.6R formulation; with increasing the transparency of the matrix phase, from Fig. 9a to c, the spatial distribution of a large number of remaining undissolved particles can be observed. The number-weighted size distribution of these particles, reveals the presence of particles up to ~130 µm equivalent spherical diameter (Fig. 9d).

Figure 9. 3D XRT image, voxel size: 1.74 µm, of a single detergent granule (equivalent diameter: 300.2 µm) produced from LW+1.6R slurry. a) – c) have increasing matrix transparency to show morphological properties and distribution of initially undissolved crystals of sodium sulphate; d) is the number based size distribution of the undissolved material.

In the 500 – 600 µm sieve fraction of the LW and LW+1.6R powders, the large central vacuole is again distinct. The size ratio of the spray-dried particle to the undissolved sodium sulphate leads to the undissolved material being distributed in the wall rather than centrally. Indeed, the extent to which undissolved particles occupy the internal space can be determined by the volume fraction of undissolved sodium sulphate within the detergent slurry and will be

similar to those estimated for the 300- 350 µm particles, see Tables 3 and 4. The presence of voids within the granule wall, as a function of the addition of sodium silicate was similarly observed for the coarse particles.

Role of sodium silicate

The presence of small voids in the wall is thought to be primarily due to the skin forming properties of sodium silicates which affects the matrix material property evolution during the puffing period of drying. The material property changes during this period of drying are important to porous structure of the dried particle (Tsotsas and Mujumdar, 2011). Aqueous sodium silicates, which are known as 'water-glasses', have a colloidal structure (Yang et al., 2008) which upon drying is known to polymerise, change from a sol to a glassy state, and form a transparent, solid, amorphous structure (Roggendorf et al., 2001). The impact of these phase changes on the rheo-mechanical properties of the silicate solution, has been observed to lead to trapped puffed structures in single drop drying experiments (Walton, 2000). The mechanical strength of the developed skin are known to determine the stability of bubbles in spray-dried particles (Both et al., 2018, Pauchard and Allain, 2003).

A secondary effect may also increase the number of trapped bubble. A reduced moisture diffusion coefficient in the silicate containing film forming materials (Walton, 2000) will restrict mass transfer and increase the droplet temperature. Consequently, in the high temperature drying conditions used, more bubbles are likely to be generated.

HW formulations

In contrast to the, LW formulations, particles produced from HW slurry show a distinctly different internal morphology, Fig. 8, with many voids forming foam-like structures. A large vacuole(s) is still observed in many particles, however, it is indistinct in a significant fraction of particles. Another key difference is that undissolved sodium sulphate crystals are rarely observed within these granules. This is to be expected due to the low fraction of undissolved sulphate anticipated, see estimates in Table 2.

Quantitative analysis of porosity and phase fractions

The volume fraction of the matrix, air, and undissolved sodium sulphate can be obtained directly from the X-ray data and are presented in Table 3. The tapped bulk density measurements and absolute density of sodium sulphate can be used to estimate the density of the matrix phase and the mass fractions of the undissolved phase present. The porosity of the matrix phase, composed of matrix solids and air pores that are less than the voxel size of 2.5 µm, can also be estimated from an estimate of the absolute density of the matrix phase, see Table 3. The mass fractions are shown in Table 4 along with the granule compositions. The small sample size X-rayed leads to a potential source of variability in the estimated values, and this needs to be considered when interpreting the data. However, the ratio of initially undissolved sulphate to that in the matrix show, is shown in Table 4, and is in good agreement with those calculated from Table 2.

The quantity and nature of the matrix phase is critical in determining the physical properties and functional performance of the product. It can be seen that even in the LW formulation which has 65% undissolved sulphate on a mass basis, the volume ratio of matrix to crystalline

sulphate is 1.66 : 1 (0.2 : 0.12), so it is the properties of the matrix which will dominate the behaviour of the granule in all respects apart from density. Comparing the LW and HW systems, a similar level of total porosity, 68% of the scanned volume being air is seen in both formulations. (This is the total of intra- and inter-granular porosity with a size > 2.5 μm, the morphology of the granules makes it very difficult to separate the contributions of intra- and inter-granular porosity.) The difference in tapped density therefore comes from the level of crystalline sodium sulphate and the lower density of the matrix (see Table 3) in the case of the HW formulation. The estimated density of the matrix is lower for the HW powder even though the absolute density of the matrix is higher (due to a higher level of inorganic material). This indicates a significantly higher matrix porosity compared to the LW case, 0.64 vs. 0.45, and gives us some insight into the sub-micron structure of these materials which is being dictated by the drying behaviour and the phase change of the matrix.

The formulations containing sodium silicate have slightly more matrix than the nil-silicate LW formulation, though interestingly, as can be seen from Table 3, the porosity of the matrix is significantly lower than both the HW and LW formulations. The level of air, is also lower in the silicate formulations, both of which lead to the higher tapped bulk density observed. The lower total porosity is thought to be due to better flowability (Farshchi et al., 2019) observed for these formulations, which leads to lower inter-particle porosity rather than any difference in large scale intra-particle porosity which as will be seen below is expected to be slightly higher than the nil-silicate LW formulation.

The influence of the initial water content and sodium silicate on the formation of bubbles can be better elucidated by distinguishing the intra-particle pores which are not connected to either the exterior or to the main central vacuole of the particle, as described in the materials and methods section. Fig. 10 shows the distribution of equivalent diameter of the intra-

particle pores obtained from the X-ray microtomography of the 300 – 350 µm powders. The smallest mean pore diameter (32.28 µm) was observed in detergent powders produced from the LW formulation. It can be observed that pore sizes are mainly distributed in a narrow range of 5-30 µm. These samples also showed the lowest pore volume fraction (φ = 4.78%). With increasing the water content (HW), a significant increase in volume of pores in a range of 30-60 µm was found which caused a shift of mean pore diameter to a larger value (46.5 µm). Furthermore, the increased water content noticeably increased the porosity to 22.81% in resulting detergent powders. This increase in porosity versus the LW formulation is far more than the overall increase in the increase in matrix mass (29.3 % for HW versus 20.3 % for LW, Table 3) and indicates that the properties of the matrix phase and increased level of water are leading to the development of the trapped pores. Comparing detergent powders containing sodium silicate, LW+1.6R and LW+2.35R, it can be observed that the pore sizes were also affected by the addition of binders. The addition of sodium silicate considerably changed the pore size distribution, the average size increased to 42.9 µm with 1.6R silicate and 46.6 µm for the 2.35R; the volume fraction of these pores is ~ 14%. Comparing to the LW formulation, the silicate is giving a higher level of closed pores and a less porous matrix, indicating a significant change in the structure of the porosity which is consistent with the material properties that would be expected from more polymeric, glassy systems discussed above.

Figure 10. Pore size distribution in spray-dried detergent powders (300-350 µm) as a function of slurry formulation. The parameters of equivalent mean void diameter (Eq. Diameter) and porosity (φ) are summarised in the graphs.

In summary, the internal morphology of the granules is driven by puffing and porosity formation which results from drying and phase transformation. As a consequence, the level of water and presence of binder lead to significant differences in the scale and structure of the porosity. This will consequently have a significant effect on detergent powder properties and performance. The complex nature of the granules makes it challenging to analyse the porosity; nevertheless, microtomography has proven to be a useful tool for quantifying aspects of the porosity and giving insight and understanding of the structures formed.

3.2.2. Microscopic observations

The complex multi-component structure of spray-dried detergent powders can be better elucidated at the micro- and nano-scale by SEM. To reveal the internal structure both fractured internal surfaces and microtome sectioned granules were analysed. Fig. 11 shows the internal surface of a fractured LW granule across a range of magnifications. At a low magnification, Fig. 11a, shows the internal surface of a fractured granule; it shows the internal surface of a large vacuole, along with fractured areas of the composite matrix. Interestingly, no obvious areas of large, originally undissolved sulphate crystals are seen. If these are present it is anticipated that they would be coated with a layer of matrix material and therefore not-necessarily obvious. In many areas of the granule the matrix is porous and several small voids distributed throughout the granule matrix.

At a higher magnification, Fig. 11b, c & d, the porous nature of the matrix is clear, the porous structure being created as the liquid phases dry, solidify and crystallize. In contrast, the granule shell, Fig.11c, appears to be more compact with limited porosity, a smooth surface and an aligned crystalline orientation within the surface layer which is of the order of a micron thick. Higher magnification analysis of the dried matrix, Fig. 11e, shows the presence of prismatic nano-sized crystals of sodium sulphate distributed within a less crystalline,

largely surfactant, continuum. The presence of these crystals was also evidenced by imaging with a back-scattered electron (BSE) detector, Fig. 11f. The brighter contrast of BSE image indicates a higher electron density region, where more electron scattering occurs, signifying the presence of sodium sulphate crystals.

Figure 11. SEM micrographs of the internal structure of a fractured detergent granule produced from LW (a – f) and HW slurries (g – i). A granule scale image of the internal surface is shown in (a), a close up view of a section of matrix and granule wall in (b), and its higher magnification image in (c). The matrix micro-structure can be observed in (d) illustrating the morphology of the porous matrix, and nano-sized crystals of sodium sulphate can be observed at its higher magnification image (e), and the same region obtained from the backscatter electron detector (f). A fractured puffed region of a HW granule is shown in (g) and higher magnification images illustrating the morphology of nano-sized crystals (h) and (i).

SEM observations of cross-sections of embedded particles also make a valuable contribution to a better understanding of the porous structure of the particles. Fig. 12 shows these for the LW, HW and LW+1.6R formulations. The porous micro-structure in these images can be classified into three groups: 1) slit-shaped closed pores, 2) irregular inter-connected open pores, < ~5 µm diameter and 3) larger, irregular semi-open macro-pores, > ~5 µm diameter. In spray-dried powders produced from LW slurry, the wall thickness is typically around 10-15 µm. The matrix of the wall appears relatively compact with slit-shaped pores, though some near spherical pores can be observed at the middle region of the wall, away from the outer shell. Interestingly, the addition of sodium silicate resulted in the formation of what looks to be relatively irregular macro-pores in the matrix. Higher water content led to the

formation of irregular open pores with some degree of interconnection within the wall of the particle. These irregular patterns might have been formed as a direct consequence of the movement and evaporation of the increased quantity of water leaving a complex structure within the matrix upon drying. The extent of pore connectivity is also evident in corresponding coloured-labelled images, showing the sets of connected pores denoted by the same colour.

Figure 12. SEM micrograph of a microtome-polished cross-section of embedded detergent powders illustrating the matrix micro-structures at high magnifications and the corresponding coloured image showing sets of connected pores labelled with the same colour, based on pixel connectivity, created by the Lable image tool in Avizo.

3.3. Surface characterization

The surface micro-structure of spray-dried detergent powders was evaluated by SEM. The micrographs in Fig. 13 show significant differences in surface morphology between the formulations. In the case of detergent granules produced from the LW formulation, the surface appears to be covered with a continuous non-crystalline matrix with a few crystallites of sodium sulphate embedded in the surface (Fig. 13b). The presence of these crystals is clearly evident in the corresponding backscattered electron micrographs (Fig. 13c). At a higher magnification some shallow folds can be observed on the surface (Fig. 13d). In contrast, HW slurry gave rise particles with a more crystalline surface. Fig. 13f, g and h illustrates that the surface morphology is mainly dominated by sub-micron sized crystals of various habits (pyramidal, dendritic and elongated).

The LW and HW formulations have virtually identical dried compositions; however, the difference in the water level in the slurries leads to the differences observed in surface morphology. Specifically, the HW formulation has a significantly higher level of sulphate in the liquid phases which dry to form the surface, see Tables 2 and 4. In the HW formulation, the sulphate is at a significantly higher level than NaLAS in the liquid phase, the sulphate:NaLAS ratio is 2.725:1, whereas in the LW formulation the sulphate is in the minority and only 0.685:1 the level of the NaLAS. Consequently, the surface of the HW system is mainly sodium sulphate, and crystalline in nature, whereas the surface in the LW formulation is mainly surfactant and virtually no crystallisation is observed.

In the powders produced from the LW+1.6R formulation the surface is relatively smooth like the LW formulation; however, there is some indication of crystallisation underneath the surface Fig. 13j and regions of crystallisation can be seen. Fig. 13 k shows elongated, almost dendritic structures, similar in the HW formulation, Fig. 13h. Areas of nano-sized crystals are also seen embedded in non-crystalline areas, Fig. 13l.

Figure. 13. Micrograph of spray-dried detergent granules. (a) A spray-dried detergent granule produced from low-water content slurries and its higher magnification image (b). (c) Shows the same region as (b) with the image obtained from a backscattered electron detector, giving larger contrast differences between the crystals and their background. A higher magnification image of the surface is shown in (d). (e) is a spray-dried HW granule; and its higher magnification surface images (f), (g) and (h). (i) is a LW+1.6R granule and its higher magnification images from a relatively smooth region (j), and its more crystalline region (k) and (l).

3.4. Bulk analysis of self-assembled nano-structures

3.4.1. Polymorphs of sodium sulphate

In the SEM micrographs, a variety of crystalline morphologies were observed, particularly on the surface of the granules. The presence of such crystal habits may arise from the existence of different polymorphs of sodium sulphate which can be examined by wide-angle X-ray scattering (WAXS). Sodium sulphate can exist in different polymorphic forms which are referred to as phase I-V. Two anhydrous polymorphs, Na_2SO_4 (V) and Na_2SO_4 (III), have been shown to crystallize out of a supersaturated solution of sodium sulphate upon evaporation among which phase V (thenardite) is considered to be the most stable anhydrous phase at room temperature (25 $^{\circ}$C). Phase III is a metastable phase which can remain stable for considerable periods of time at typical room temperatures and humidities. However, this polymorph may undergo a transition to phase V at humidities above its deliquescence humidity, *e.g*. RH >83.5% at 25 ºC (Rodriguez-Navarro et al., 2000). Other polymorphic forms of sodium sulphates, *i.e*. I, II and IV, are considered as high-temperature polymorphs and there has been no precedent for the presence of these polymorphs at near ambient temperature (Rodriguez-Navarro et al., 2000, Linnow et al., 2006).

The thenardite (phase V) crystal lattice is thought to be built from parallel chains consisting of SO_4 tetrahedra and deformed NaO_6 octahedra at which isolated sulphates share two of their edges with the octahedra. The other corners of each octahedron are shared with four sulphate ions giving rise an orthorhombic unit cell (Kamburov et al., 2014). This structure gives rise to a bipyramidal crystal shape. Although phase III similarly consists of orthorhombic unit cells, its structure is thought to be built up from deformed tetrahedral and octahedral chains. In this

crystal structure there are two types of NaO_6 in terms of Na-O distances, which connect to each other with a common face (Rasmussen et al., 1996, Vidya and Lakshminarasappa, 2013). This results in a orthorhombic lattice having different cell dimensions than the unit cells in thenardite, and a distinct difference in crystal morphology.

In this study all the detergent powders exhibited well-defined, sharp diffraction peaks which are characteristic of the well-ordered crystal lattices of phase III and V forms of sodium sulphate (Fig. 14).

Figure 14. Wide-angle X-ray scattering (WAXS) patterns of the spray-dried powders showing the presence of phase III and phase V sodium sulphate.

The XRD patterns in Fig. 14, revealed the presence of thenardite (phase V) as the only polymorph in detergent powders produced from the LW slurry. For LW formulations the XRD pattern would be expected to be dominated by the structure of the undissolved sodium sulphate particles present in the slurry. The single polymorph observed in this case indicates that crystallisation from the matrix, both in the bulk and at the surface, results in the phase V form. However, either increasing the amount of water or adding sodium silicate gave rise to the formation of the metastable phase III. This is clearly seen by the splitting of a diffraction peak at 23.2° 2Θ and the emergence of two new peaks at 25.6 and 37.9° 2Θ which are characteristics in a change in lattice parameters from thenardite (phase V) to phase III (Rodriguez-Navarro et al., 2000). The emergence of new peaks was also accompanied by the increased intensity of phase III peaks overlapping with thenardite at 31.85° and 33. 86° 2Θ.

The growth of phase III crystals, from binary solutions of sodium sulphate and water, has been suggested to be due to spontaneous nucleation (Mehrotra, 1981). Rodriguez-Navarro et al. (2000) reported that non-equilibrium morphologies of these crystals are indicative of slightly higher evaporation rates and/or higher supersaturation ratios, both of which are consistent with spray drying. In the current study, the crystallization of phase III seen in the HW formulation might be explained by faster evaporation conditions which occur as a result of the lower LAS concentration in the matrix phase, alternatively the crystallisation may be directly affected by the composition and material properties of the matrix.

Phase III was also similarly observed in XRD patterns of detergent powders containing sodium silicate. A likely explanation for this is the adsorption of negatively charged silicate species on intermediate clusters of sodium sulphate, thereby regulating the nucleation and growth of sodium sulphate crystals. The interaction between negatively charged additives and sodium sulphate nuclei has been previously reported by Ruiz-Agudo et al. (2006) who showed pH was a factor in determining the relative growth rate of thernadite and mirabilite polymorphs. Silicate species are known to have a strong tendency to adsorb onto a variety of surfaces of metal oxides and clays. It has been shown that dissolved silica species can affect both the nucleation and crystal growth of inorganic minerals (Anderson and Benjamin, 1985, Gal et al., 2010). In the early stage of crystallization, silicate species can modify the rate and extent of cluster aggregation, *i.e.* nucleation, by shielding the positively charged precursors. During growth, these anions can adsorb on specific faces, thereby regulating the growth rate of these faces, consequently this changes the crystal habit (Kellermeier et al., 2013, Ruiz-Agudo et al., 2006). Therefore, a possible reason for the presence of phase III in silicate-containing detergent powders can be due to the adsorption of negatively charged silicate ions on the positively charged precursors (existing as small amorphous particles) of sodium sulphate and potentially also on their growth and final crystal habit

The results of X-ray diffraction measurements are consistent with the microscopic observations which show the presence of dendritic crystals on the granule surface for HW and silicate-containing formulations but not the LW formulation. The morphologies of the observed tiny branched crystals (Fig. 13h and k), which consist of elongated needles assembled as dendrites, were roughly consistent with those of phase III, as previously reported by others (Rodriguez-Navarro et al., 2000). Although both phases III and V were identifiable by means of scanning electron microscopy, on the surface of the detergent granules (Fig. 13), it is more difficult to identify phase III within the internal structure of the granules (Fig. 11).

Reviewing Fig. 11, in the context of the WAXS results, the nano-sized crystals, crystallised from the matrix of both the LW and HW formulations, have a broadly similar morphology, and an apparent planar or lamellar character. (The higher sodium sulphate to LAS ratio in the HW matrix being responsible for the higher fraction of clearly visible crystals observed versus the LW system.) In the HW system the multitude of bipyramidal prisms are typical of the morphology of thenardite (phase V) (Atzeni et al., 1995, Vidya and Lakshminarasappa, 2013). The nano-crystals in the LW formulations perhaps show a slightly more elongate habit versus the HW system, Fig. 11e,f.

3.4.2. Phase behaviour of surfactant (NaLAS) molecules

Amphiphilic molecules are known to have a tendency to arrange themselves, in the presence of water, into various ordered nano-structures (1, 2 and 3 dimensional self-assemblies) depending on their concentration and molecular shape. While the formation of micellar

structures is favoured at concentrations equal to or greater than critical micellar concentration (CMC), higher concentrations may give rise to the formation of disk-like or rod-like micelles, hexagonal, cubic and particularly liquid crystalline phases (Israelachvili, 2011, Kulkarni et al., 2011). Aqueous NaLAS systems show this typical phase behaviour, though typically no hexagonal phase is observe in the phase diagram *e.g.* Liaw et al. (2003); Richards et al. (2009) and Stewart et al. (2009). The addition of electrolytes to low concentration aqueous surfactant solutions is known to 'salt out' the surfactant. Stewart et al. (2011) have shown this for NaLAS where the addition of electrolyte leads to the formation of a concentrated liquid crystalline surfactant phase. The phase behaviour of self-assembled structures of NaLAS is of significant interest due to its potentially significant effect on the physical properties, *e.g.* flowability, dissolution rate and physical stability, of laundry powders.

A SAXS study revealed the presence of multiple lamellar phases in the spray-dried powders. Fig. 15 shows that up to four Bragg diffraction peaks were present, with the first-order reflection peaks showing lamellar *d*-spacings between ~26 and 43 Å. The largest *d*-spacings (43.0 Å) can be seen in the LW and HW formulation, though the intensity of the peaks related to the two larger *d*-spacings were noticeably reduced in the HW powders. These reductions in *d*-spacing intensities signify a decrease in population of the corresponding lamellar phases (Bolze et al., 2000). A reduced coherence and size of the liquid crystalline domains within the crystallised matrix is also likely as the level of sub-micron sulphate crystallites is significantly higher in the HW powders.

Interestingly, the disappearance of relatively long-periodicities in the presence of sodium silicate, led to a more uniform system with stronger Bragg peaks. The detergent powders containing sodium silicate LW+1.6R and LW+2.35R, show a remarkable similarity in the

number of coexisting lamellar polymorphs, indicating the silicate ratio has no effect on the self-assembled surfactant structure.

Figure 15. Bragg diffraction peaks fitted to SAXS patterns of the four spray-dried powders studied. The colours correspond to equivalent peaks in each powder.

The occurrence of coexisting lamellar phases of NaLAS in liquid detergent systems has been previously reported by Richards et al. (2009) and Stewart et al. (2009), which, according to the authors, was attributed to the natural heterogeneity of the chemical structure of NaLAS. It was suggested that NaLAS isomers possessing a benzene ring substituted in the middle of hydrocarbon chain, *i.e. v*-shaped isomers, trigger the formation of lamellar phases, while NaLAS isomers with a benzene ring at the extremities of the hydrocarbon chain, but not terminal $–CH_3$, promote the formation of micellar phases. Richards et al. (2007) attributed the occurrence of multiple lamellar phases to the local segregation of different NaLAS positional isomers, possessing different alkyl chain length, within the bilayers, which subsequently swell to different extents upon exposing to elevated temperatures. Liaw et al. (2003) showed that the addition of sodium silicate with the SiO_2:Na_2O molar ratios of 2.0 to NaLAS pastes, gives rise to the formation of more spherical and tightly packed multi-lamellar vesicles. These structural changes in NaLAS paste were concomitant with a reduction in lamellar *d*-spacing which is in good agreement with the SAXS results presented here. Nevertheless, the nature of these structural changes in lamellar phase remains an interesting problem which merits future investigation.

3.5. Conclusion

The structure of spray-dried detergent powders can be described as a solid multi-component colloidal system where sub-micron crystals of inorganic salts along with dried lamellar liquid crystals of NaLAS form a continuous porous matrix in which large sulphate crystals, which were originally undissolved in the slurry, and air vacuoles and voids are dispersed. It was shown that the initial water content of the slurries play a crucial role in determining the matrix composition and micro-structure of the resulting detergent powders. This was seen in the proportion of remaining undissolved sodium sulphate and in the matrix composition. The greater the initial slurry water content, the greater the ratio of dissolved sodium sulphate to NaLAS within the matrix. This increase in sulphate concentration lead to changes in the internal matrix micro-structure and was also reflected in the surface composition and micro-structure, where a more crystalline surface was observed.

The addition of binders, *i.e.* sodium silicates, and the amount of initial water content of the slurries governed the morphological properties at a particle scale. The increased water content resulted in the formation of agglomerated, blistered particles. These powders also showed the largest mean particle size (377 μm). On the contrary, near spherical particles were produced from low-water content slurries, though some surface agglomeration, the adhesion of fine particles on the surface of larger parent granules, was observed upon the addition of sodium silicates.

Spray-dried powders produced from low-water content slurries are either hollow or semi-solid. In the latter case, remaining undissolved sodium sulphate occupies most of the internal space of the granules as a large crystallite. The hollow structures were particularly observed in coarse particles in which undissolved sodium sulphate crystals are distributed around a large central vacuole. The addition of sodium silicate changed the nature of the porous structure and voids were observed within the walls of the hollow granules. The internal

structure; however, became noticeably different once the initial water content of the slurries increased to 63.0 wt%. This resulted in the formation of foam-like structures, at the macro-scale, where a central vacuole is not always encountered. At the micro-scale, the influence of the increased water content was evident from the micrographs of microtome-polished detergent powders which showed irregular connected pores within the matrix.

The dispersed nano-structures, *i.e.* sodium sulphate polymorphs and lamellar liquid crystalline phases, were shown to be influenced by the initial chemical composition of the slurries. The WAXS results showed that both increased water content and the addition of sodium silicate result in the formation of metastable polymorphs of sodium sulphate (phase III). The SAXS results showed the presence of several co-existing liquid crystalline phases, similar to those seen by previous investigators in similar aqueous systems (not dried powders). It was found that the addition of sodium silicate leads to a more uniform lamellar phase with a narrower range of *d*-spacings. The level of water in the slurry was also observed to have a significant effect on the SAX scattering from the powders produced from them; the same peaks being present but the higher water contents leading to a significant reduction in peak intensity suggesting less coherence in liquid crystalline domains. These interesting SAXS results merit future investigation.

Even in these simple model systems, the complexity of the structure is evident. Simple changes such as the amount of water in the slurry, which does not affect the final particle composition, can have a significant effect on the structure across multiple scales, and consequently the properties and performance of the detergent compositions will be altered in perhaps non-obvious ways. This highlights the challenges for scientists and engineers who are developing and optimising both formulations and production processes and seeking to maximise product performance for a given cost. The link between structure, properties and

performance has not been addressed by this study and also needs to be understood and quantified; this will be the subject of further studies on these systems.

ACKNOWLEDGEMENT

The authors would like to thank the Advanced Manufacturing Supply Chain Initiative (AMSCI) [grant number 31587, 233189] for funding the project. AMSCI is a government supply chain fund which is helping to rebuild British manufacturing processes. We also acknowledge the input of Sam Tantawy, Joel Caragay and Paul Gould of Procter and Gamble for production of materials and their support throughout the project.

References

ALI, M., MAHMUD, T., HEGGS, P. J., GHADIRI, M., BAYLY, A., AHMADIAN, H. & MARTIN DE JUAN, L. 2017. CFD modeling of a pilot-scale countercurrent spray drying tower for the manufacture of detergent powder. *Drying Technology,* 35**,** 281-299.

ANDERSON, P. R. & BENJAMIN, M. M. 1985. Effect of silicon on the crystallization and adsorption properties of ferric oxides. *Environmental Science & Technology,* 19**,** 1048-1053.

ANSARI, M. A. & STEPANEK, F. 2008. The effect of granule microstructure on dissolution rate. *Powder Technology,* 181**,** 104-114.

ASAY, D. B. & KIM, S. H. 2005. Evolution of the Adsorbed Water Layer Structure on Silicon Oxide at Room Temperature. *The Journal of Physical Chemistry B,* 109**,** 16760-16763.

ATZENI, C., CABIDDU, M. G., MASSIDDA, L. & SANNA, U. 1995. Crystallization of sodium sulphate in polymer impregnated plasters. *Cement and Concrete Composites,* 17**,** 3-8.

BLEI, S. & SOMMERFELD, M. Lagrangian modelling of agglomeration during spray drying processes. Proceedings of the 9th International Conference on Liquid Atomization and Spray Systems, 2003. 13-17.

BOEREFIJN, R., DONTULA, P.-R. & KOHLUS, R. 2007. Chapter 14 Detergent granulation. *Handbook of Powder Technology,* 11**,** 673-703.

BOLZE, J., FUJISAWA, T., NAGAO, T., NORISADA, K., SAITÔ, H. & NAITO, A. 2000. Small angle X-ray scattering and 31P NMR studies on the phase behavior of phospholipid bilayered mixed micelles. *Chemical Physics Letters,* 329**,** 215-220.

BOTH, E. M., KARLINA, A. M., BOOM, R. M. & SCHUTYSER, M. A. I. 2018. Morphology development during sessile single droplet drying of mixed maltodextrin and whey protein solutions. *Food Hydrocolloids,* 75**,** 202-210.

BRAGG, W. H. & BRAGG, W. L. 1913. The reflection of X-rays by crystals. *Proceedings of the Royal Society of London. Series A, Containing Papers of a Mathematical and Physical Character,* 88**,** 428-438.

CHARLESWORTH, D. H. & MARSHALL, W. R. 1960. Evaporation from drops containing dissolved solids. *AIChE Journal,* 6**,** 9-23.

FRANCIA, V., MARTÍN, L., BAYLY, A. E. & SIMMONS, M. J. H. 2015. Particle Aggregation in Large Counter-current Spray Drying Towers: Nozzle Configuration, Vortex Momentum and Temperature. *Procedia Engineering,* 102**,** 668-675.

FRANCIA, V., MARTÍN, L., BAYLY, A. E. & SIMMONS, M. J. H. 2016a. Agglomeration in counter-current spray drying towers. Part A: Particle growth and the effect of nozzle height. *Powder Technology,* 301**,** 1330-1343.

FRANCIA, V., MARTÍN, L., BAYLY, A. E. & SIMMONS, M. J. H. 2016b. Agglomeration in counter-current spray drying towers. Part B: Interaction between multiple spraying levels. *Powder Technology,* 301**,** 1344-1358.

GAL, A., WEINER, S. & ADDADI, L. 2010. The Stabilizing Effect of Silicate on Biogenic and Synthetic Amorphous Calcium Carbonate. *Journal of the American Chemical Society,* 132**,** 13208-13211.

GAMBLE, J. F., TERADA, M., HOLZNER, C., LAVERY, L., NICHOLSON, S. J., TIMMINS, P. & TOBYN, M. 2016. Application of X-ray microtomography for the characterisation of hollow polymer-stabilised spray dried amorphous dispersion particles. *International Journal of Pharmaceutics,* 510**,** 1-8.

GOULA, A. M. & ADAMOPOULOS, K. G. 2008. Effect of Maltodextrin Addition during Spray Drying of Tomato Pulp in Dehumidified Air: II. Powder Properties. *Drying Technology,* 26**,** 726-737.

GRIFFITH, J. D., BAYLY, A. E. & JOHNS, M. L. 2007. Evolving micro-structures in drying detergent pastes quantified using NMR. *Journal of Colloid and Interface Science,* 315**,** 223-229.

HAFID, H., OVARLEZ, G., TOUSSAINT, F., JEZEQUEL, P. H. & ROUSSEL, N. 2016. Effect of particle morphological parameters on sand grains packing properties and rheology of model mortars. *Cement and Concrete Research,* 80**,** 44-51.

HECHT, J. P. & KING, C. J. 2000. Spray Drying: Influence of Developing Drop Morphology on Drying Rates and Retention of Volatile Substances. 1. Single-Drop Experiments. *Industrial & Engineering Chemistry Research,* 39**,** 1756-1765.

ISRAELACHVILI, J. N. 2011. *Intermolecular and surface forces: revised third edition*, Academic press.

JUPPO, A. M. & YLIRUUSI, J. 1994. Effect of amount of granulation liquid on total pore volume and pore size distribution of lactose, glucose and mannitol granules. *European journal of pharmaceutics and biopharmaceutics,* 40**,** 299-309.

KAMBUROV, S., SCHMIDT, H., VOIGT, W. & BALAREW, C. 2014. Similarities and peculiarities between the crystal structures of the hydrates of sodium sulfate and selenate. *Acta Crystallographica Section B,* 70**,** 714-722.

KELLERMEIER, M., GLAAB, F., KLEIN, R., MELERO-GARCIA, E., KUNZ, W. & GARCIA-RUIZ, J. M. 2013. The effect of silica on polymorphic precipitation of calcium carbonate: an on-line energy-dispersive X-ray diffraction (EDXRD) study. *Nanoscale,* 5**,** 7054-7065.

KULKARNI, C. V., WACHTER, W., IGLESIAS-SALTO, G., ENGELSKIRCHEN, S. & AHUALLI, S. 2011. Monoolein: a magic lipid? *Physical Chemistry Chemical Physics,* 13**,** 3004-3021.

LEROCH, S. & WENDLAND, M. 2012. Simulation of Forces between Humid Amorphous Silica Surfaces: A Comparison of Empirical Atomistic Force Fields. *The Journal of Physical Chemistry C,* 116**,** 26247-26261.

LI, R. F., PENCHEV, R., RAMACHANDRAN, V., ROBERTS, K. J., WANG, X. Z., TWEEDIE, R. J., PRIOR, A., GERRITSEN, J. W. & HUGEN, F. M. 2008. Particle Shape Characterisation via Image Analysis: from Laboratory Studies to In-process Measurements Using an in Situ Particle Viewer System. *Organic Process Research & Development,* 12**,** 837-849.

LINNOW, K., ZEUNERT, A. & STEIGER, M. 2006. Investigation of Sodium Sulfate Phase Transitions in a Porous Material Using Humidity- and Temperature-Controlled X-ray Diffraction. *Analytical Chemistry,* 78**,** 4683-4689.

MEHROTRA, B. N. 1981. The crystal structure of Na_2SO_4 III. *Zeitschrift für Kristallographie - Crystalline Materials,* 155**,** 159-163.

OKORAFOR, O. C. 1999. Solubility and Density Isotherms for the Sodium Sulfate−Water−Methanol System. *Journal of Chemical & Engineering Data,* 44**,** 488-490.

PAUCHARD, L. & ALLAIN, C. 2003. Buckling instability induced by polymer solution drying. *EPL (Europhysics Letters),* 62**,** 897.

RASMUSSEN, S. E., JORGENSEN, J.-E. & LUNDTOFT, B. 1996. Structures and Phase Transitions of Na2SO4. *Journal of Applied Crystallography,* 29**,** 42-47.

RICHARDS, C., MOHAMMADI, M. S. & TIDDY, G. J. T. 2009. Formulating liquid detergents with naturally derived surfactants—Phase behaviour, crystallisation and rheo-stability of primary alkyl sulphates based on coconut oil. *Colloids and Surfaces A: Physicochemical and Engineering Aspects,* 338**,** 119-128.

RICHARDS, C., TIDDY, G. J. T. & CASEY, S. 2007. Lateral Phase Separation Gives Multiple Lamellar Phases in a "Binary" Surfactant/Water System: The Phase Behavior of Sodium Alkyl Benzene Sulfonate/Water Mixtures. *Langmuir,* 23**,** 467-474.

RODRIGUEZ-NAVARRO, C., DOEHNE, E. & SEBASTIAN, E. 2000. How does sodium sulfate crystallize? Implications for the decay and testing of building materials. *Cement and Concrete Research,* 30**,** 1527-1534.

ROGGENDORF, H., BÖSCHEL, D. & TREMPLER, J. 2001. Structural evolution of sodium silicate solutions dried to amorphous solids. *Journal of Non-Crystalline Solids,* 293-295**,** 752-757.

ROUQUEROL, F., ROUQUEROL, J. & SING, K. 1999. CHAPTER 1 - Introduction. *Adsorption by Powders and Porous Solids.* London: Academic Press.

RUIZ-AGUDO, E., RODRIGUEZ-NAVARRO, C. & SEBASTIÁN-PARDO, E. 2006. Sodium Sulfate Crystallization in the Presence of Phosphonates: Implications in Ornamental Stone Conservation. *Crystal Growth & Design,* 6**,** 1575-1583.

STEWART, J. A., SAIANI, A., BAYLY, A. & TIDDY, G. J. T. 2009. The phase behaviour of lyotropic liquid crystals in linear alkylbenzene sulphonate (LAS) systems. *Colloids and Surfaces A: Physicochemical and Engineering Aspects,* 338**,** 155-161.

STEWART, J. A., SAIANI, A., BAYLY, A. & TIDDY, G. J. T. 2011. Phase Behavior of Lyotropic Liquid Crystals in Linear Alkylbenzene Sulphonate (LAS) Systems in the Presence of Dilute and Concentrated Electrolyte. *Journal of Dispersion Science and Technology,* 32**,** 1700-1710.

TSOTSAS, E. & MUJUMDAR, A. S. 2011. *Modern drying technology: Volume 3, Product quality and formulation,* Weinheim; Chichester, Wiley-VCH.

ULUSOY, U. & KURSUN, I. 2011. Comparison of different 2D image analysis measurement techniques for the shape of talc particles produced by different media milling. *Minerals Engineering,* 24**,** 91-97.

VAN DALEN, G., NOOTENBOOM, P. & HEUSSEN, P. C. M. 2011. Correlative microscopy of detergent granules. *Journal of Microscopy,* 241**,** 273-281.

VERDURMEN, R. E. M., MENN, P., RITZERT, J., BLEI, S., NHUMAIO, G. C. S., SONNE SØRENSEN, T., GUNSING, M., STRAATSMA, J., VERSCHUEREN, M., SIBEIJN, M., SCHULTE, G., FRITSCHING, U., BAUCKHAGE, K., TROPEA, C., SOMMERFELD, M., WATKINS, A. P., YULE, A. J. & SCHØNFELDT, H. 2004. Simulation of Agglomeration in Spray Drying Installations: The EDECAD Project. *Drying Technology,* 22**,** 1403-1461.

VIDYA, Y. S. & LAKSHMINARASAPPA, B. N. 2013. Preparation, Characterization, and Luminescence Properties of Orthorhombic Sodium Sulphate. *Physics Research International,* 2013**,** 7.

WALTON, D. E. 2000. THE MORPHOLOGY OF SPRAY-DRIED PARTICLES A QUALITATIVE VIEW. *Drying Technology,* 18**,** 1943-1986.

WALTON, D. E. 2002. Spray-Dried Particle Morphologies. *Developments in Chemical Engineering and Mineral Processing,* 10**,** 323-348.

WALTON, D. E. & MUMFORD, C. J. 1999. The Morphology of Spray-Dried Particles: The Effect of Process Variables upon the Morphology of Spray-Dried Particles. *Chemical Engineering Research and Design,* 77**,** 442-460.

YANG, X., ROONASI, P. & HOLMGREN, A. 2008. A study of sodium silicate in aqueous solution and sorbed by synthetic magnetite using in situ ATR-FTIR spectroscopy. *Journal of Colloid and Interface Science,* 328**,** 41-47.

Table 1. Composition of the detergent slurry formulations

	Compositions of the detergent slurries (wt %)				
Description	Water	NaLAS	Sodium Sulphate	Sodium Silicate (1.6 R)	Sodium Silicate (2.35 R)
LW	30.0	13.6	56.4		
HW	63.0	7.2	29.8		
LW+1.6R	28.0	14.0	49.3	8.6	
LW+2.35R	28.0	14.0	47.2		10.8

Table 2. Estimated composition of the phases in detergent slurries used

Description	Sodium sulphate in detergent slurries (wt %)			Estimated compositions of the liquid phases in detergent slurries (wt %)				
	Undissolved Sodium Sulphate	Dissolved Sodium Sulphate	Undissolved/Dissolved Ratio	Water	NaLAS	Sodium Sulphate	Sodium Silicate (1.6 R)	Sodium Silicate (2.35 R)

LW	47.1	9.3	5.1	56.7	25.7	17.6		
HW	10.3	19.5	0.53	70.2	8.0	21.8		
LW+1.6R	40.6	8.7	4.7	47.2	23.6	14.6	14.5	
LW+2.35 R	38.5	8.7	4.4	45.5	22.8	14.1		17.6

Table 3. Volume composition and phase densities of detergent powders, 300 – 350 µm fraction

Description	Tapped bulk density (kg/m^3)	Volume fraction (vol %)			Matrix Density (kg/m^3)	Est. Abs Density of Matrix (kg/ m^3)	Matrix Porosity
		Air	Matrix	Undissolved Sodium Sulphate			
LW	472	0.68	0.20	0.12	791	1430	0.45
HW	267	0.68	0.29	0.02	696	1915	0.64
LW+1.6R	544	0.62	0.27	0.11	888	1421	0.37
LW+2.35R	536	0.63	0.28	0.10	1005	1464	0.31

Table 4. Composition of the resulting detergent powders (200 – 350 um), calculated from X-ray microtomography analysis

Description	Approximate compositions of the detergent powders (wt %)					
	Moisture	NaLAS	Dissolved Sodium Sulphate	Undissolved Sodium Sulphate	Sodium Silicate	Mass Ratio undissolved:dissolved
LW	0.5	19.5	15.26	65.24		4.28
HW	1.0	19.5	57.3	23.2		0.40
LW+1.6R	2.0	19.5	11.9	56.6	12.0	4.76
LW+2.35R	1.2	19.5	14.3	51.2	15.0	3.58

Notes: Moisture contents were determined using a gravimetric method, *i.e.* dynamic vapour sorption (DVS). The quantities of undissolved sodium sulphate were measured using x-ray microtomography.

Graphical abstract:

Highlights

- The complex multi-scale structure of spray dried detergent formulations is revealed
- Structure consists of inorganic crystallites and vacuoles bound by porous matrix
- Sub-micron sodium sulphate crystals are embedded in the surfactant, binder matrix
- Formulation changes affect structures across all scales; nano - colloidal - particle
- Slurry water content plays a key role in structure and therefore properties